J Solid State Electrochem (2010) 14:579–583
DOI 10.1007/s10008-009-0813-6

ORIGINAL PAPER

Effect of the cathode structure on the electrochemical performance of anode-supported solid oxide fuel cells

Junliang Li · Shaorong wang · Zhenrong Wang · Jiqin Qian · Renzhu Liu · Tinglian Wen · Zhaoyin Wen

Received: 21 December 2008 / Revised: 12 February 2009 / Accepted: 20 February 2009 / Published online: 6 March 2009

Abstract The study elementarily investigated the effect of the cathode structure on the electrochemical performance of anode-supported solid oxide fuel cells. Four single cells were fabricated with different cathode structures, and the total cathode thickness was 15, 55, 85, and 85 μm for cell-A, cell-B, cell-C, and cell-D, respectively. The cell-A, cell-B, and cell-D included only one cathode layer, which was fabricated by $(La_{0.74}Bi_{0.10}Sr_{0.16})MnO_{3-\delta}$ (LBSM) electrode material. The cathode of the cell-C was composed of a $(La_{0.74}Bi_{0.10}Sr_{0.16})MnO_{3-\delta} - (Bi_{0.7}Er_{0.3}O_{1.5})$ (LBSM–ESB) cathode functional layer and a LBSM cathode layer. Different cathode structures leaded to dissimilar polarization character for the four cells. At 750°C, the total polarization resistance (R_p) of the cell-A was 1.11, 0.41 and 0.53 Ω cm^2 at the current of 0, 400, and 800 mA, respectively, and that of the cell-B was 1.10, 0.39, and 0.23 Ω cm^2 at the current of 0, 400, and 800 mA, respectively. For cell-C and cell-D, their polarization character was similar to that of the cell-B and R_p also decreased with the increase of the current. The maximum power density was 0.81, 1.01, 0.79, and 0.43 W cm^{-2} at 750°C for cell-D, cell-C, cell-B, and cell-A, respectively. The results demonstrated that cathode structures evidently influenced the electrochemical performance of anode-supported solid oxide fuel cells.

Keywords Anode-supported solid oxide fuel cells · Cathode structure · Impedance spectroscopy

J. Li · S. wang (✉) · Z. Wang · J. Qian · R. Liu · T. Wen · Z. Wen
Shanghai Institute of Ceramics, Chinese Academy of Sciences,
1295 Dingxi Road,
Shanghai 200050, People's Republic of China
e-mail: srwang@mail.sic.ac.cn

Introduction

The solid oxide fuel cell (SOFC) is a promising power generation device [1–3] since it provides high electrical conversion efficiency exceeding 50%. In order to reach a basis for commercial viability, SOFC must reduce its operating temperature. A lower operating temperature involves several advantages such as the use of cheaper materials for interconnects and manifolds, reduced sealing and corrosion problems, and increased lifetime and reliability. However, the power output of SOFC systems is rebated at lower operating temperatures. So, it is necessary to use other materials for the electrolyte and electrode or optimize processing and microstructure parameters of existing SOFCs. It is reported that a significant improvement in the cell performance can be achieved by investigating new cathodes' materials [4–10]. In comparison with the performance of cathodes based on LSM, LSCF cathodes are very excellent. For example, LSCF cathodes gave a power output of 1.0–1.2 W cm^{-2} at 800°C and 0.7 V with hydrogen as fuel gas: Compared with conventional cathodes based on LSM, the high power densities allow a reduction in operating temperatures of about 100°C by maintaining the same performance [4]. Besides, the addition of small amounts of noble metals, e.g., Pd, Ag, or Pt, to the cathode can also improve the electrochemical performance of electrodes [11–18]. In the other hand, studies have already been initiated in order to develop different cathode microstructures and fabrication methods [19–23]. Sasaki et al. found that the best thickness of a LSM cathode was 20 μm and suggested that the performance of cathodes was closely related to the length of the triple phase boundary [24]. To improve the electrochemical performance of LSM-based anode-supported single cells, the geometrical parameters of the cathode functional layer

and cathode current collector layer were investigated in detail, as described [25].

The study was designed to examine the effect of the LBSM cathode structure on the electrochemical performance of anode-supported solid oxide fuel cells. The analysis focused on the characterization of the cell performance according to different cathode designs.

Experimental

Anode-supported electrolyte film was fabricated by tape casting procedure, as reported [26]. Commercial NiO (Inco, Canada) was used with 8 mol% yttria-stabilized ZrO_2 (YSZ, TOSOH, Japan) powder for preparing the substrate and with scandia-stabilized zirconia, $Zr_{0.89}Sc_{0.1}Ce_{0.01}O_{2-x}$ (SSZ, Daiichi Kigenso Kagaku Kogyo, Japan), for the anode functional layer. The ratio of the mixtures (NiO–YSZ, NiO–ScSZ) was 50 wt.% of NiO and 50 wt.% of stabilized zirconia. The SSZ powder was also used to prepare the electrolyte film. The powders of these functional layers were ball-milled with organic additives to form slurries, which were assembled together with the multilayer tape casting procedure to get the green tapes. After dryness, the green tape was co-sintered at 1,400 °C for 4 h in air to get the anode-supported SSZ film.

LBSM ($(La_{0.74}Bi_{0.10}Sr_{0.16})MnO_{3-\delta}$) powder was synthesized by autoignition of citrate–nitrate gel, and ESB ($Bi_{0.7}Er_{0.3}O_{1.5}$) powder was synthesized by the conventional solid state reaction, as described [27]. LBSM–ESB50 mixtures were prepared by mixing the LBSM powder with an equal amount of ESB. Pastes for the screen-printing process to apply the cathode layers (or cathode functional layers) were prepared by mixing the LBSM (or LBSM–ESB50) powder with a binder consisting of ethyl cellulose in terpineol, then they were screen-printed onto the anode-supported SSZ film and sintered at 900 °C for 2 h to form the cathode. Cell-A, cell-B, and cell-D were prepared with the LBSM cathode, and cell-C was fabricated with the LBSM–ESB50 cathode functional layer and LBSM cathode layer on anode-supported SSZ film. The cathode area was around 1.33 cm^2 for performance test. Platinum mesh, attached to the cathode surface with platinum paste, was used as the current collector and platinum wire as lead.

The microstructure of the cell was examined by scanning electron microscopy (SEM, JXA-8100, JEOL, Japan). The cell performance and AC impedance spectroscopy were measured at different temperatures with humidified H_2 (a water content of around 3 vol.%) as the fuel and oxygen as the oxidant. The cell current–voltage (I–V) curves were tested at a scanning rate of 10 mV S^{-1}. The impedances were measured in the frequency range of 1 MHz–0.03 Hz with excitation potential of 20 mV. A four-probe configuration was adopted in the electrochemical testing.

Results and discussion

Microstructure

Figure 1 shows the cross-section SEM images of cathodes with different thickness on the anode-supported SSZ film. As shown in Fig. 1, the electrodes showed typical porous microstructure and a uniform, continuous, and quite dense SSZ electrolyte was achieved and with a thickness of around 15 μm. As shown in Fig. 1a–d, the thickness of the electrode layers was around 15, 55, 85, and 85 μm for cell-A, cell-B, cell-C, and cell-D, respectively. The electrode of the cell-C consisted of a cathode functional layer with a thickness of around 30 μm and a cathode layer with a thickness of around 55 μm. It could be seen that the size of the LBSM particles in cathode layers was about 400 nm in diameter in Fig. 1a–d and that of the ESB particles in the cathode functional layer was about 1 μm as shown in Fig. 1c.

For solid oxide fuel cells, oxygen is reduced at the cathode and the interface of the cathode and electrolyte. Although the triple phase boundary (TPB) at the electrolyte/cathode is a main location for the reduced reaction of oxygen, the porous cathode is also very important for the absorption and decomposition of oxygen. Cell-A, cell-B, and cell-D were prepared by the identical process, so the size scale of the LBSM particles and pores in the cathode were basically identical, and the length of the TPB at the electrolyte/cathode was also equal by and large. For cell-A, the thickness of its cathode was only 15 μm. In other words, the effective area for the absorption and decomposition of oxygen was smaller than that of the cell-B with a relatively thick cathode (around 55 μm). Therefore, the difference in cathode thickness might explain why cell-B showed higher electrochemical performance than cell-A since more surface area was available for the absorption of oxygen into the cathode structure of cell B, which was beneficial to the electrochemical reaction of the cathode. Further, the thickness of electrode layers in cell-C and cell-D was about 85 μm, but a cathode functional layer (around 30 μm) was introduced into cell-C, which extended the total effective length of TPB and contributed to a higher cell performance.

Polarization behavior

Figure 2a–d shows impedance diagrams measured with a variety current at 750 °C for cell-A, cell-B, cell-C, and cell-D, respectively. The variation in the trend of the cell-A polarization resistance (R_p) was different from that of the cell-B, cell-C, and cell-D as the increase of the current. At

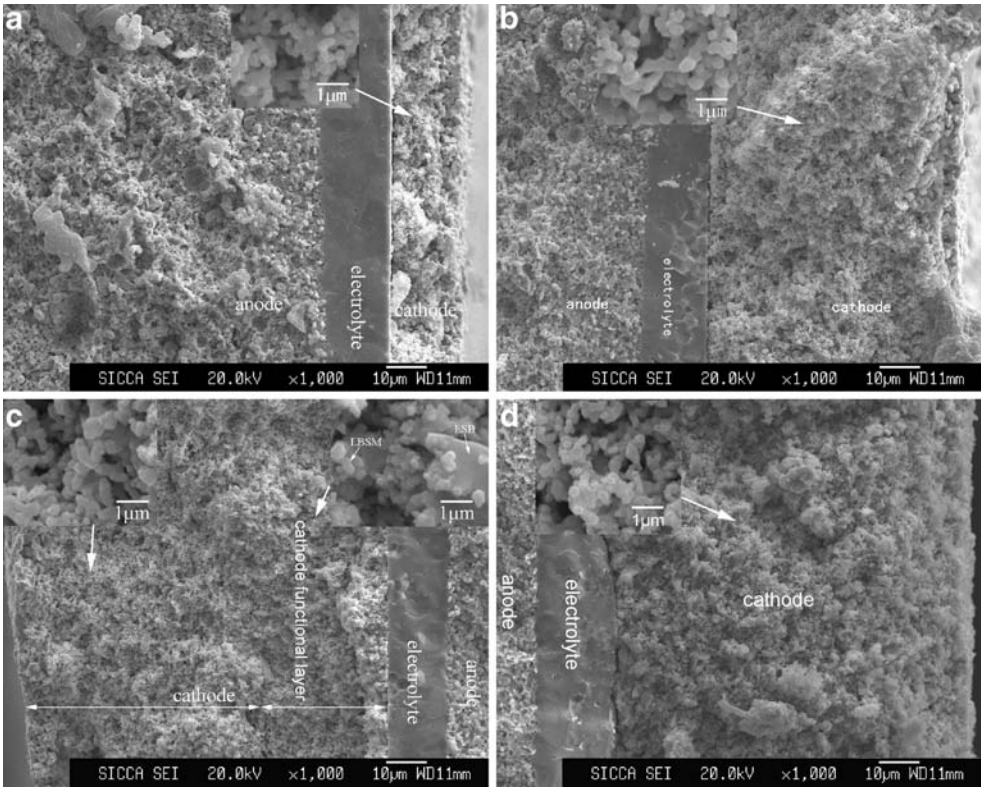

Fig. 1 Typical fracture cross-section SEM images of the cell-A (**a**), cell-B (**b**), cell-C (**c**), and cell-D (**d**)

750 °C, the cell-A yielded R_p=1.11, 0.41, and 0.53 Ω cm^2 at the current of 0, 400, and 800 mA; the cell-B yielded R_p= 1.10, 0.39, and 0.23 Ω cm^2 at the current of 0, 400 and 800 mA; the cell-C yielded R_p=0.46, 0.31, and 0.19 Ω cm^2 at the current of 0, 400, and 800 mA; and the cell-D yielded R_p=1.09, 0.37, and 0.21 Ω cm^2 at the current of 0, 400, and 800 mA, respectively. For the above four cells, the anodic and electrolyte resistances could be reasonably assumed

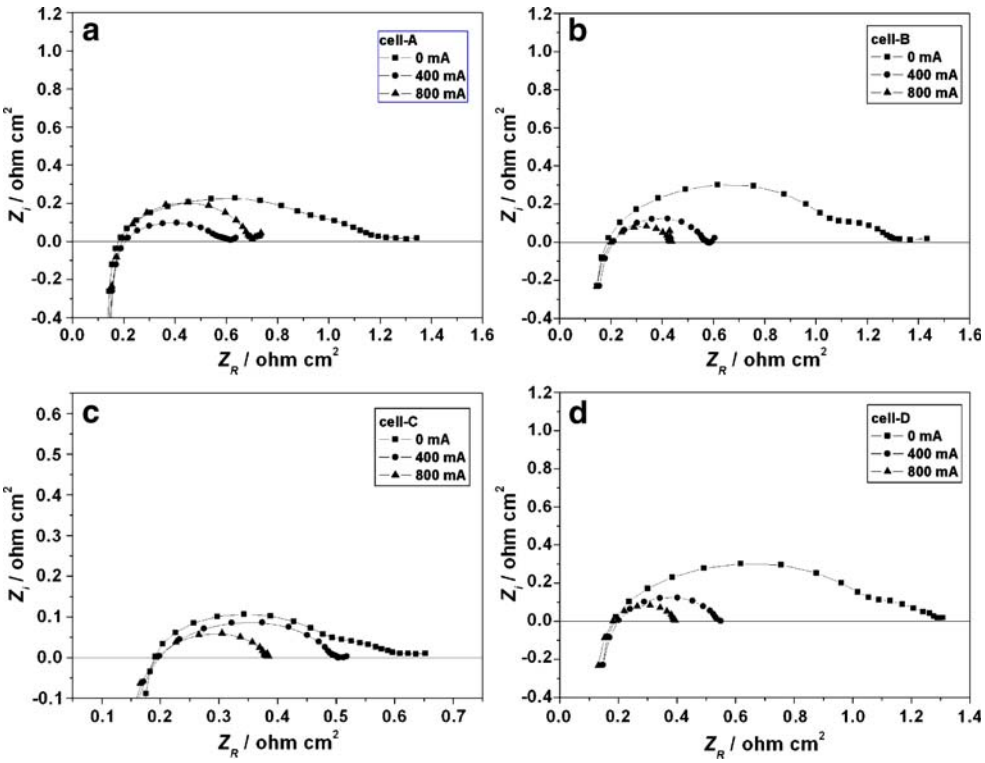

Fig. 2 AC impedance diagrams measured with a variety current at 750 °C for cell-A (**a**), cell-B (**b**), cell-C (**c**), and cell-D (**d**)

identical because the anode and electrolyte were fabricated with the same procedures. So, the different polarization behavior resulted from the dissimilar structures of cathodes.

For cell-A and cell-B, R_p was approximative when the current was 0 and 400 mA. However, when the current increased to 800 mA, R_p for cell-A increased to 0.53 Ω cm^2 while R_p for cell-B decreased to 0.23 Ω cm^2. The results suggested that the effect of the thickness of cathodes on the polarization resistance was not obvious when the current density through the cells was lower, and the effect became evident as a further increase of the current. This effect might be a result of the difference in the effective area for the absorption and decomposition of oxygen in cathodes with various thickness. Based on the formula proposed by van Heuveln and Bouwmeester [28], the reaction model for oxygen reduction on the cathode is given as follows.

Model:

Step 1. $O_{2(g)} \rightarrow 2O_{ad}$
Step 2. $O_{2(g)} + e' \rightarrow O_{ad'}$
Step 3. $O_{ad'} \rightarrow O_{TPB'}$
Step 4. $O_{TPB} + e' \rightarrow O_{TPB''}$
Step 5. $O_{TPB''} + Vo^{\cdot\cdot} \rightarrow O_{o^x}$

The electrochemical reaction in cathodes needs more O_{TPB} as an increase of the current, so step 3 is the pivotal reaction. In other words, more adsorbed oxygen (O_{ad}) is necessary as an increase of the current. In this way, thick electrodes are beneficial to the absorption and decomposition of oxygen and the process of the electrochemical reaction (steps 1 and 2). So, cell-B had a lower resistance than cell-A. A cathode functional layer was introduced into cell-C, which effectively extended the length of the TPB, and the location for the exchange of oxygen was evidently increased. So, cell-C had more active area for the electrochemical reaction, and its R_p was obviously lower than that of the cell-A and cell-B. The cathode thickness of the cell-D was equal with that of the cell-C, but there was not a cathode functional layer in cell-D. R_p was approximative under the same conditions for cell-B and cell-D, and R_p for cell-D was higher than cell-C. In other words, it is not necessary to blindly increase the thickness of the electrode. It was reported that the cathode layer having a thickness of 50–60 μm was enough for single cells [25]. However, the cathode functional layer in cell-C is beneficial to the decrease of the polarization resistance.

Cell performance

The performance evaluation of cells in this study was carried out by anode-supported single cells with SSZ film as electrolyte. Figure 3 shows the current voltage characteristics and the corresponding power densities for four fuel cells. They were measured at different temperatures with humidified hydrogen (a water content of around 3 vol.%) as the fuel and oxygen as the oxidant. As shown in Fig. 3a, the maximum power densities were 0.43, 0.79, and 1.01 W cm^{-2} at the same temperature (750°C) for cell-A, cell-B, and cell-C, respectively. The maximum power densities increased with the increase of the cathode thickness. For cell-A, its voltage decreased abruptly when the current density was over 0.71 A cm^{-2}, which could be due to an increase in the concentration polarization. The cathode of cell-A could

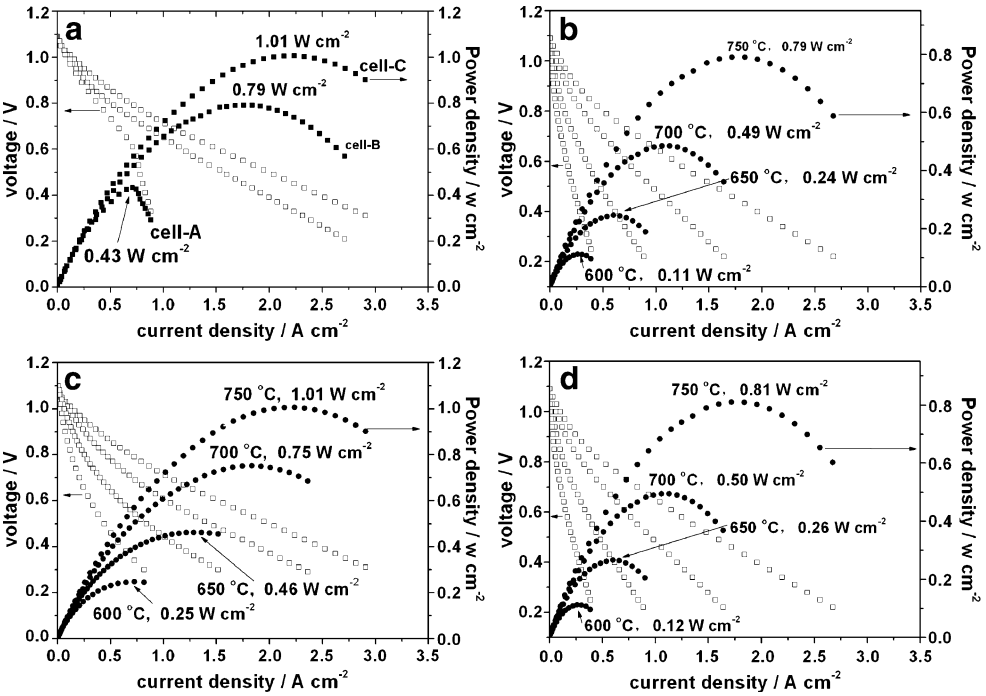

Fig. 3 The cell voltage and power density as a function of current density of the three cells measured at 750 °C (**a**), the cell-B (**b**), cell-C (**c**), and cell-D (**d**) operating at various temperatures

not absorb enough oxygen for the electrochemical reaction at a relatively high current density because its thickness is too thin (around 15 μm), and the effective area for the absorption and decomposition of oxygen was not enough. As shown in Fig. 3b–d, the maximum power densities (MPD) for cell-B were 0.11, 0.24, and 0.49 W cm^{-2} at 600, 650, and 700°C; the MPD for cell-C were 0.25, 0.46, and 0.75 W cm^{-2} at 600, 650, and 700°C; and the MPD for cell-D were 0.12, 0.26, and 0.50 W cm^{-2} at 600, 650, and 700°C, respectively. The performance of the cell-C with a cathode functional layer was obviously higher than that of the cell-B and cell-D under the same conditions, and the high power densities allowed a reduction in operating temperatures of about 50°C by maintaining the same performance. The length of the TPB was further extended in the cathode functional layer, which could effectively enhance the oxygen reduction reaction and further improve the performance of the cell-C. For the above four cells, the anodic and electrolyte resistances could be reasonably assumed identical because the anode and electrolyte were fabricated with the same procedures. So, the relatively higher power densities resulted from the higher performance of cathodes. It demonstrated that the fabrication and thickness of cathodes had a significant effect on the absorption and decomposition of oxygen as well as the cell performance.

It should be noted that the thickness of the cathode layer can significantly influence the overall electrochemical performance of solid oxide fuel cells. In addition, the cathode functional layer is also very useful in improving the cell performance. So, the design of cathodes is important for solid oxide fuel cells. Further study should be performed to optimize the thickness of two different layers, including the cathode layer and the cathode functional layer, and control the size ratio of two different particles in the cathode functional layer for improving the cell performance.

Conclusion

Results from electrochemical measurements showed that the performance of LBSM-based solid oxide fuel cells can be improved by optimizing the fabrication and thickness of cathodes. For example, at 750°C, the total polarization resistance of the cell-A with a thin cathode (around 15 μm) was 0.53 Ω cm^2 at the current of 800 mA and that of the cell-B and cell-D with the thick cathodes was 0.23 and 0.21 Ω cm^2 at the same current. For cell-C, including a cathode function layer (around 30 μm) and a cathode layer (around 55 μm), its total polarization resistance reduced to 0.19 Ω cm^2 at the current of 800 mA. Besides, the maximum power densities were 0.81, 1.01, 0.79, and 0.43 W cm^{-2} at 750°C for cell-D, cell-C, cell-B, and cell-A, respectively. The results also demonstrated that the LBSM-based cathode is a very promising cathode material for intermediate-temperature solid oxide fuel cells.

Acknowledgment This work is supported financially by the Chinese High Technology Development Project (2007AA05Z151).

References

1. Ujiie T (2007) ECS Trans 7:3. doi:10.1149/1.2729066
2. Surdoval WA (2007) ECS Trans 7:11. doi:10.1149/1.2729067
3. Rietveld B (2007) ECS Trans 7:17. doi:10.1149/1.2729068
4. Mai A, Haanappel VAC, Uhlenbruck S, Tietz F, Stover D (2005) Solid State Ion 176:1341. doi:10.1016/j.ssi.2005.03.009
5. Tietz F, Haanappel VAC, Mai A, Mertens J, Stover D (2006) J Power Sources 156:20. doi:10.1016/j.jpowsour.2005.08.015
6. Murray EP, Sever MJ, Barnett SA (2002) Solid State Ion 148:27. doi:10.1016/S0167-2738(02)00102-9
7. Tu HY, Takeda Y, Imanishi N, Yamamoto O (1999) Solid State Ion 117:277. doi:10.1016/S0167-2738(98)00428-7
8. Yamamoto O, Takeda Y, Kanno R, Noda M (1987) Solid State Ion 22:241. doi:10.1016/0167-2738(87)90039-7
9. Jiang SP, Wang W (2005) Solid State Ion 176:1351. doi:10.1016/j.ssi.2005.03.011
10. Tsai T, Barnett SA (1997) Solid State Ion 98:191. doi:10.1016/S0167-2738(97)00113-6
11. Erning JW, Hauber T, Stimming U, Wipperman K (1996) J Power Sources 61:205. doi:10.1016/S0378-7753(96)02358-0
12. Wang S, Kato T, Nagata S, Kaneko T, Iwashita N, Honda T, Dokiya M (2002) Solid State Ion 152:477. doi:10.1016/S0167-2738(02)00376-4
13. Sahibzada M, Benson SJ, Rudkin RA, Kilner JA (1998) Solid State Ion 113:285. doi:10.1016/S0167-2738(98)00294-X
14. Wang S, Kato T, Nagata S, Honda T, Kaneko T, Iwashita N, Dokiya M (2002) Solid State Ion 146:203. doi:10.1016/S0167-2738(01)01015-3
15. Sasaki K, Tamura J, Dokiya M (2001) Solid State Ion 144:233. doi:10.1016/S0167-2738(01)00972-9
16. Watanabe M, Uchida H, Shibata M, Mochizuki N, Amikura K (1994) J Electrochem Soc 141:342. doi:10.1149/1.2054728
17. Uchida H, Yoshida M, Watanabe M (1999) J Electrochem Soc 146:1. doi:10.1149/1.1391555
18. Sasaki K, Tamura J, Hosoda H, Lan TN, Yasumoto K, Dokiya M (2002) Solid State Ion 148:551. doi:10.1016/S0167-2738(02)00116-9
19. Tsai T, Barnett SA (1997) Solid State Ion 93:207. doi:10.1016/S0167-2738(96)00524-3
20. Jørgensen MJ, Primdahl S, Mogensen M (1999) Electrochim Acta 44:4195. doi:10.1016/S0013-4686(99)00134-6
21. Juhl M, Primdahl S, Manon C, Mogensen M (1996) J Power Sources 61:173. doi:10.1016/S0378-7753(96)02361-0
22. Hart NT, Brandon NP, Day MJ, Lapena-Rey N (2002) J Power Sources 106:42. doi:10.1016/S0378-7753(01)01035-7
23. Lee YK, Kim JY, Lee YK, Kim I, Moon HS, Park JW, Jacobson CP, Visco SJ (2003) J Power Sources 115:219. doi:10.1016/S0378-7753(02)00727-9
24. Sasaki K, Wurth JP, Gschwen R, Godickemeier K, Gauckler LJ (1996) J Electrochem Soc 143:530. doi:10.1149/1.1836476
25. Haanappel VAC, Mertens J, Rutenbeck D, Tropartz C, Herzhof W, Sebold D, Tietz F (2005) J Power Sources 141:216. doi:10.1016/j.jpowsour.2004.09.016
26. Wang ZR, Qian JQ, Cao JD, Wang SR, Wen TL (2007) J Alloy Comp 437:264. doi:10.1016/j.jallcom.2006.07.110
27. Li JL, Wang SR, Wang ZR, Liu RZ, Wen TL, Wen ZY (2008) J Power Sources 179:474. doi:10.1016/j.jpowsour.2008.01.017
28. Van Heuveln FH, Bouwmeester HJM (1997) J Electrochem Soc 144:134. doi:10.1149/1.1837375